

VERY LARGE SPAN OPENINGS AT SHALLOW DEPTH:
DEFORMATION MAGNITUDES FROM JOINTED MODELS
AND F.E. ANALYSIS

by Nick Barton and Harald Hansteen

Norwegian Geotechnical Institute, Oslo, Norway.

The deformations resulting from excavation of very large openings are compared using two-dimensional F.E. continuum analyses and discontinuous physical models (20,000 discrete blocks). Both the joint orientations and the model horizontal stress levels were varied. Some models were dynamically loaded to simulate earthquakes (0.2-0.7 g). Model deformations were recorded using photogrammetry. The changes in deformation when increasing the simulated spans from 20 m to 50 m were of particular interest. High horizontal stress caused surface heave when joint orientations were favourable for arch stability. Joint orientations also determined whether the pillars between parallel openings were in a state of compression or tension.

INTRODUCTION

The engineering performance of large rock caverns has traditionally been learned from mining and hydro power projects, where the depth below surface is often many times greater than the span of the openings. Deformations measured in the walls and roofs of hydro power caverns generally range from about 5-50 mm, though there is a documented case where a wall moved in 126 mm (1), and another where the arch moved down 147 mm (2).

The chief objectives of the present studies of large near-surface openings were threefold:

- (i) to provide deformation data to compare with monitored data from planned engineering projects involving large span near-surface excavations, e.g. underground sports complexes, civil defense shelters, nuclear power stations,

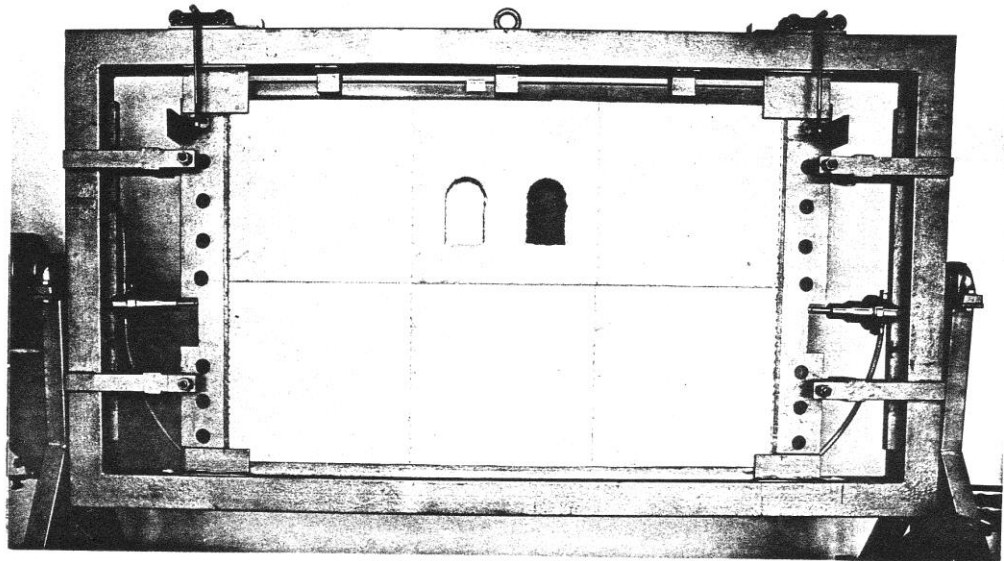
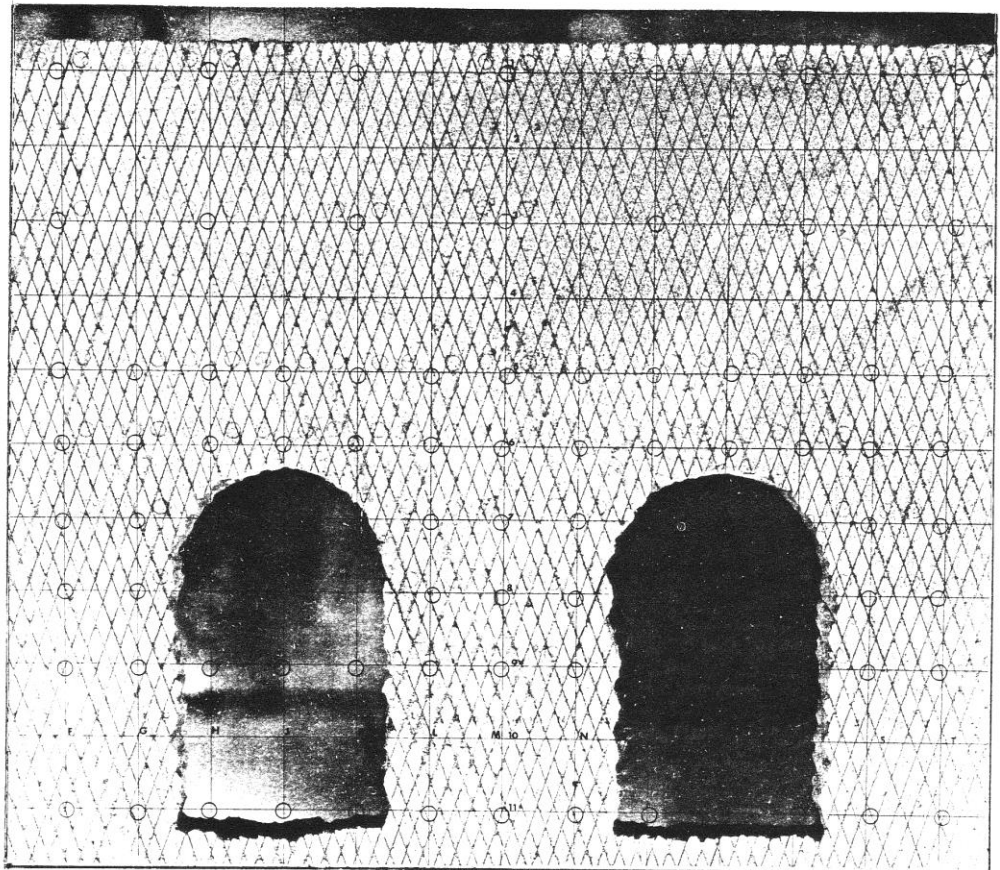


Fig. 1 Model in loading frame, and detail of joints (below).



- (ii) to try to evaluate the extent to which linear elastic continuum analyses are able to model the response of near-surface excavations in jointed rock (3),
- (iii) to provide a physical check (validation) for some sophisticated numerical modelling that is in progress in several countries, in which jointing is simulated (4, 5, 6).

For these reasons the strength-displacement properties of individual model joints and of the model rock mass are given in some detail, so that input data can be formulated.

SIMULATION OF A ROCK MASS

A complete discussion on the derivation of scaling laws by dimensional analysis would exceed the scope of this paper (7). It will be sufficient to point out here that to satisfy the relationship between strength scaling, geometric scaling and density in a gravity loaded model, the model material must have high density and low strength.

In this study a geometric scale (λ) of 1:300 was adopted. This made it possible to simulate horizontal dimensions of approximately 350 metres and a depth of approximately 250 metres in a model measuring 120 by 80 cm (see Figure 1). The present model was "two-dimensional", having a wall thickness of 25 mm. It was loaded under *plane stress* conditions. The ratio of prototype and model densities was approximately 1.33 (25/19). Thus the stress scale (ψ) was 1:400 (equation 1).

1. Properties of intact model material.

The model material consists of a mixture of red lead-sand-ballotini-plaster-water. This is poured into 400x400x25 mm moulds. The set slabs are cured in an oven at 105°C. The physical properties of a range of these weak brittle materials have been described in detail previously (7). Table 1 summarizes some of the present model-prototype values:

$$\psi = \lambda \cdot \rho_r / \rho_m \quad \dots\dots\dots (1)$$

TABLE 1. Properties of material C8 used in the present models.

SYMBOL	MODEL	UNITS	PROTOTYPE
σ_c	0.44	Mpa	175
σ_c / σ_t	8 (approx.)	-	8 (approx.)
E (intact)	87	Mpa	35 000
ρ	19	kN/m ³	25

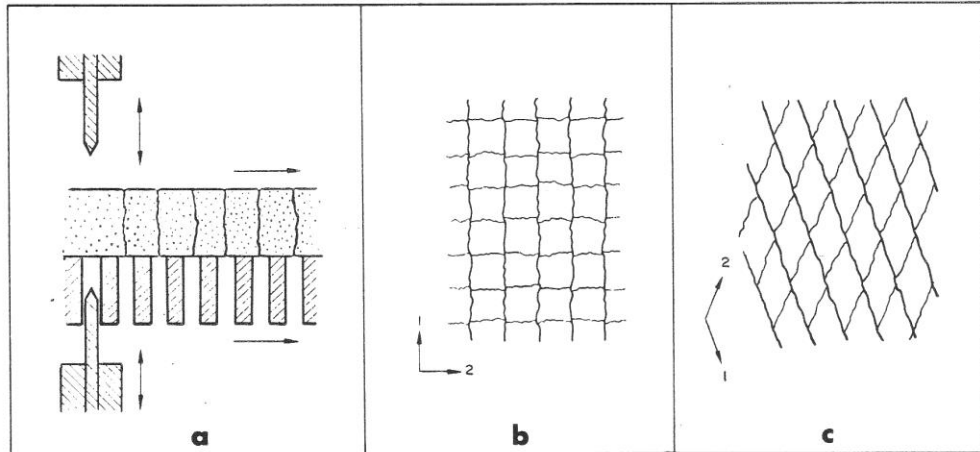


Fig. 2. (a) Principle of guillotine operation.
 (b) Offset secondary joints, orthogonal sets.
 (c) Down-stepping secondary joints, conjugate sets.

2. Properties of model joints.

Rough interlocking tension fractures are generated in 25 mm thick slabs of the model material using a double bladed "guillotine" (8). The principle is illustrated in Figure 2. An important and realistic feature of this fracture formation is that the *primary* joints (those first developed) are the only continuous unstepped fractures. Joints of the *secondary* set are offset where they intersect the "older" primary joints.

The shear strength envelopes obtained from shear box tests performed on 100 mm long model joints under a realistic range of model normal stresses are shown in Figure 3. The peak strength (τ) of these *primary* joints is described closely by equation 2. A significant portion of this peak strength is due to the dilation that accompanies shearing of these rough joints (9).

$$\tau = \sigma_n \tan [JRC \log_{10} (JCS/\sigma_n) + \phi_r] \quad \dots\dots\dots(2)$$

where

JRC = joint roughness coefficient = 20

JCS = joint wall compression strength = 0.44 Mpa
 (JCS = σ_c since no weathering)

$\phi_r = 30^\circ$

The secondary joints have additional shear strength due to the cohesion caused by orthogonal offsets (Figure 2b), and due to a direction dependent geometric component (i) in the case of the conjugate

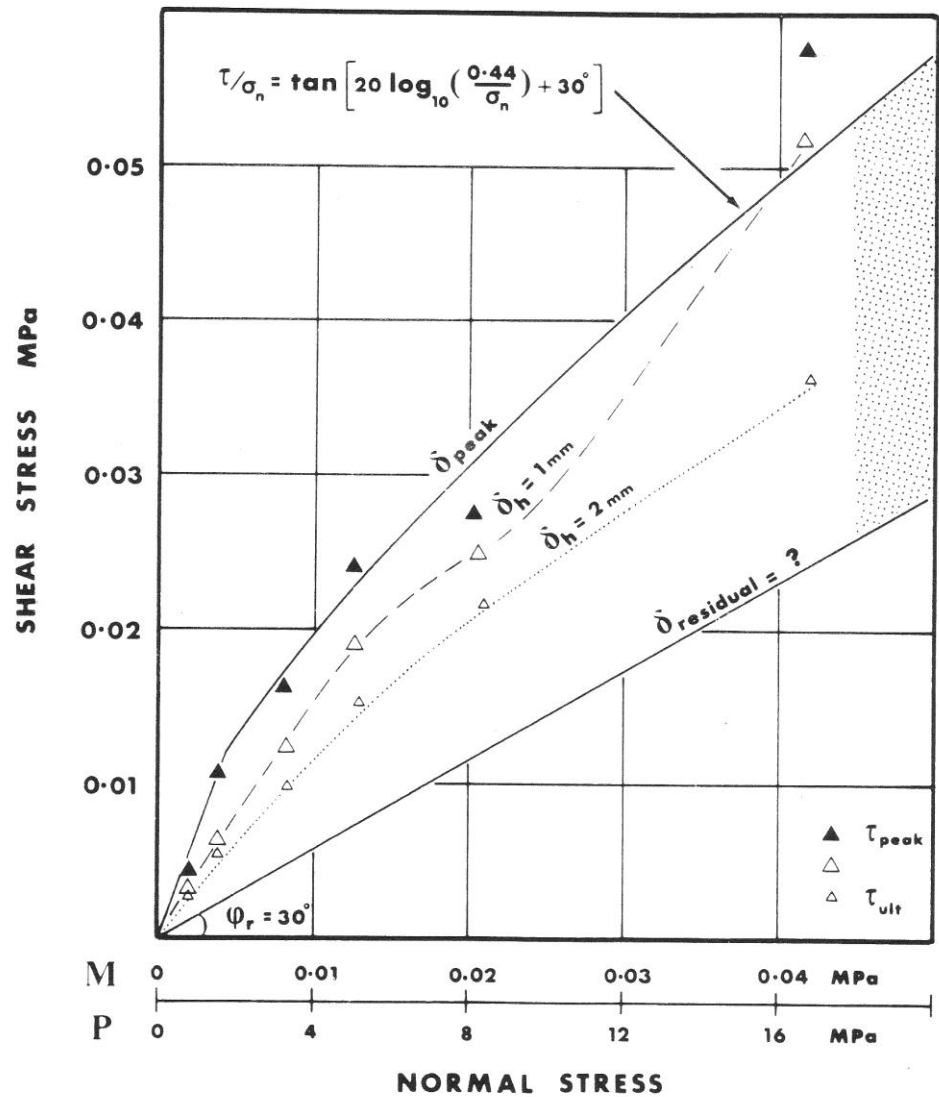


Fig. 3. Shear strength envelopes for 100 mm long primary joints. M represents model normal stress, P represents prototype normal stress. (Stress scale $\Psi = 1:400$).

joints (Figure 2c). The latter can be added to ϕ_r since it is probably independent of σ_n .

The shear force-displacement curves obtained from these shear tests are plotted in dimensionless form in Figure 4. Equation 2 was evaluated along each shear force-displacement curve in order to back-

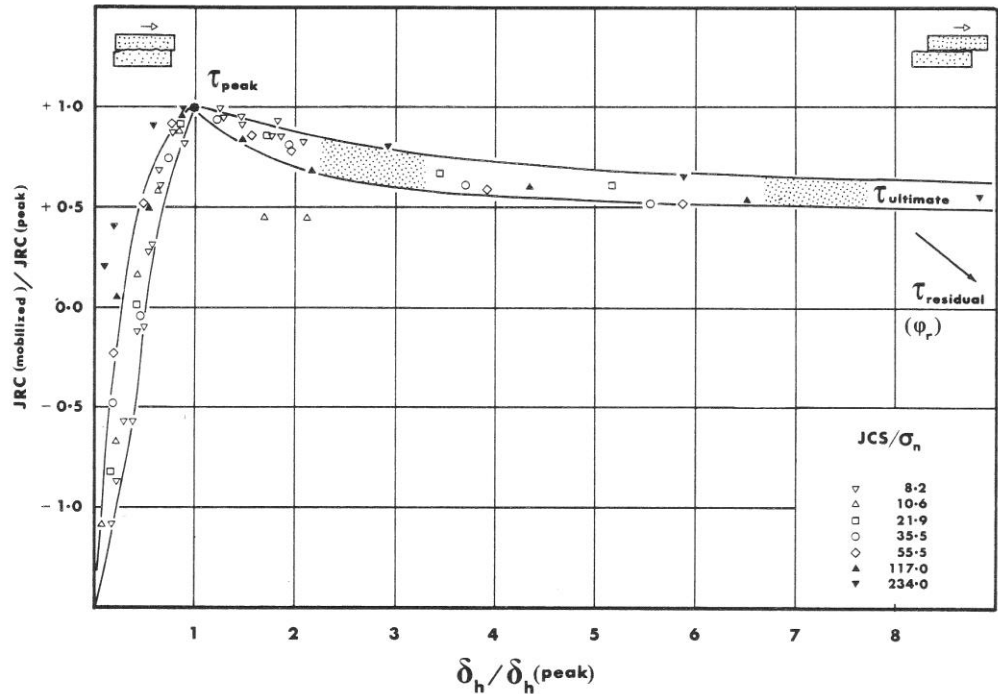


Fig. 4. Shear strength - displacement behaviour (dimensionless).

calculate JRC (mobilized). At *peak-strength* JRC (mob.) is equal to JRC (peak), and δ_h (instantaneous horizontal shear displacement) is equal to δ_h (peak). The scatter of data in Figure 4 is due to the range of values of JCS/σ_n .

This method of representing joint behaviour forms the basis of a simplified constitutive law for rock joints. Table 2 indicates how it can be used to numerically formulate shear behaviour. An important aspect of this method is that different loading paths or loading histories can be followed. This is important when attempting to formulate the effects of unloading (excavation) on a jointed rock mass.

The results of *normal loading* tests on *primary* model joints are shown in Figure 5. Behaviour is hysteretic, with different stiffnesses governing loading and unloading. This is an important feature of rock mass behaviour, and is responsible for some of the differences between *discontinuum* and *continuum* behaviour.

3. Properties of the model rock mass.

The hypothetical model rock mass E modulus can be calculated from equation 3, assuming deformation across only one set of joints (8).

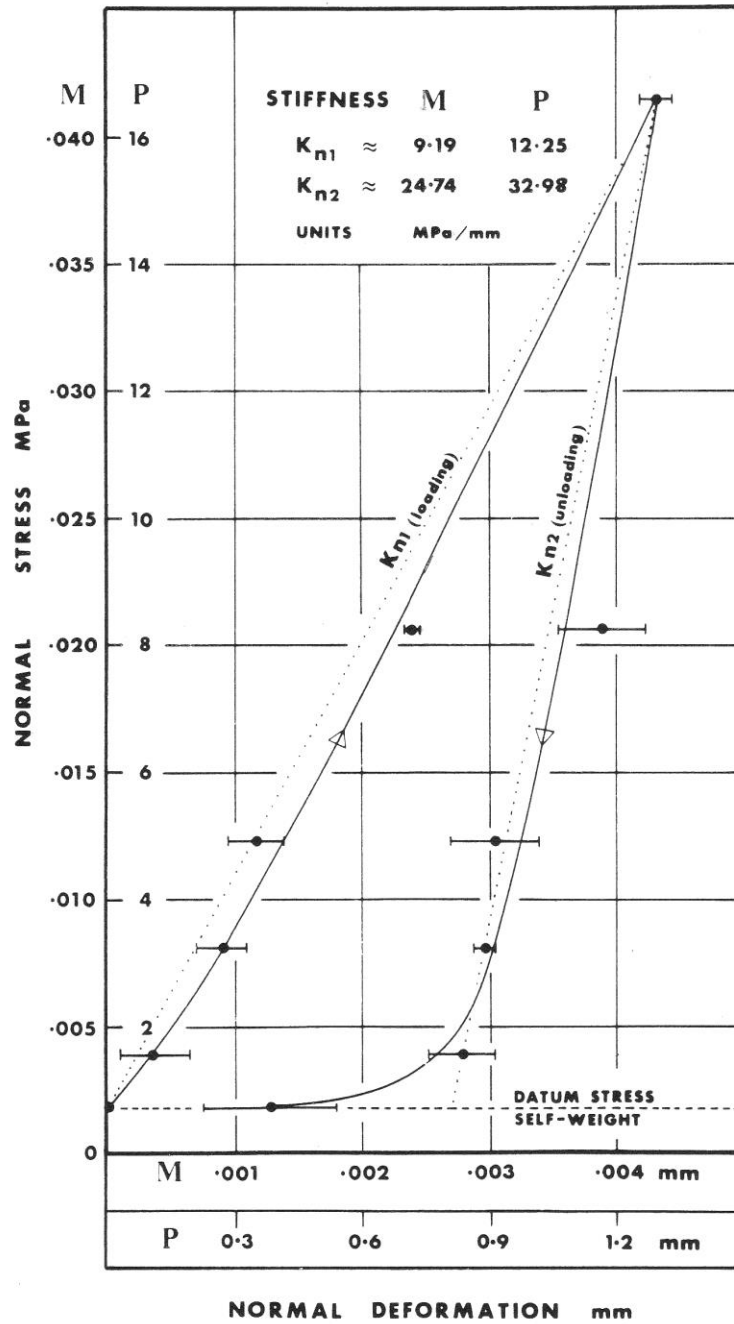


Fig. 5. Normal stiffness of model primary joints. Model (M) and prototype (P) values are given. Scale factor = Ψ/λ (=400/300)

TABLE 2. Simplified constitutive law for rock joints.

$\delta_h/\delta_h(\text{peak})$	JRC (mob.)/JRC (peak)
0	$-\phi/i$ (origin, Fig.4)
0.5	0.5
1.0 (ϕ peak)	1.0
2.5	0.75
10 (ϕ ultimate)	0.5
100 (ϕ residual)	0

where $i = \text{JRC} \cdot \log_{10} (\text{JCS}/\sigma_n)$. ϕ *ultimate* is the usual limit of most shear tests. ϕ *residual* is not reached until much larger displacements, here assumed as $100 \delta(\text{peak}) \approx$ the length of joint (L) since $\delta(\text{peak}) \approx 1/100 L$ (see (9)).

$$E_m/E_i = \left[\frac{K_n \cdot S}{K_n \cdot S + E_i} \right] \dots\dots\dots (3)$$

where E = deformation modulus of model rock mass
 E_m = deformation modulus of intact model material
 S^i = mean joint spacing

For the case of the model the joint spacing was 6 mm, or 1.8 m at prototype scale. Table 3 gives the appropriate model and prototype values of deformation moduli. These values are probably of most relevance to the deformation moduli obtained from plate loading or flat jack tests where only joints of one set are significantly loaded. Values of E_m may be significantly lower when all sets are involved, some in shear.

TABLE 3. Hypothetical isotropic E moduli of the model rock mass.

SYMBOL	MODEL	UNITS	PROTOTYPE
LOADING			
E_m	34.9	MPa	14,000
E_m/E_i	0.40	-	0.40
UNLOADING			
E_m	55.9	MPa	22,500
E_m/E_i	0.64	-	0.64

A parallel series of *plane stress* biaxial tests on jointed slabs measuring 400x400x25 mm (containing 250, 1000 or 4000 blocks each) indicated that for certain joint orientations, deformation moduli could be as low as 4100-7500 MPa (at prototype scale, loading). Two other important findings from the biaxial tests were as follows:

- (i) Model rock masses composed of differently spaced joints (6, 12

or 24 mm) have different JRC values despite identical roughness. In other words reduced block size is found to increase the shear strength due to reduced mass stiffness and increased degree of freedom. Small blocks "follow" all scales of roughness more readily. The usual scale effect on JRC described by Barton and Choubey (9) may therefore be reversed in model studies, the 100 mm long model shearbox samples were *too long* to represent the jointed mass.

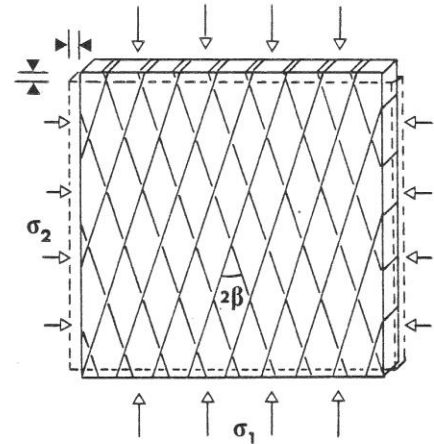


Table 4 indicates the scale effect involved. For the case of the primary joints, an appropriate value of JRC would appear to be 26 for the small block sizes studied, not 20 as suggested earlier.

TABLE 4. Shear strength scale effect due to JRC dependence on block size or joint length.

BLOCK SIZE OR JOINT LENGTH MODEL	JRC PROTOTYPE	JRC at peak	TYPE OF TEST
60,100 mm	18,30 m	20.0 (mean)	Shear box
40 mm	12 m	21.6	Biaxial
20 mm	6 m	25.1	"
10 mm	3 m	26.7	"
6 mm	1.8 m	26.0	"

- (ii) Model rock masses loaded in shear demonstrate a marked "psuedo" Poisson's ratio effect due to joint deformation (both shear and dilation). The ratio of lateral strain/axial strain increases to well beyond 0.5 as shear strength is increasingly mobilized. Table 5 indicates typical values obtained from a series of biaxial tests with the included angle 2β ranging from 36° to 45° . Models with 250, 1000 and 4000 blocks all gave similar results.

A related feature of jointed rock masses (or jointed models) that distinguishes discontinuum and continuum behaviour is the anisotropic stiffness. The peak *shear stiffness* (K_s) of a jointed rock mass can be approximated by the following equation (9).

$$K_s = \frac{100}{L_c} \cdot \sigma_n \tan [JRC \log_{10} (JCS/\sigma_n) + \phi_r] \dots\dots\dots(4)$$

where L_c = cross-joint spacing (or effective block size)

TABLE 5. Effect of mobilized shear strength on volume change measured in biaxial tests on jointed models.

$\tau(\text{mob.})/\tau(\text{peak})$	$\epsilon(\text{lateral})/\epsilon(\text{axial})$	JRC(mob.)/JRC(peak)	
0.3	0.1	- 1.0	
0.4	0.2	- 0.5	
0.45	0.3	0	
0.5	0.4	+ 0.25	See
0.65	0.6	+ 0.50	Fig.4
0.85	1.0	+ 0.75	
1.0(peak)	2.0(local failures)	+ 1.0	

The range of prototype block sizes simulated (1.8 or 3.0 m) and the range of normal stress levels simulated (approx. 1-15 MPa), suggests values of K_S approximately in the range 0.1-1.0 MPa/mm according to equation 4. Comparison of these values with the *normal stiffness* K_n given in Figure 5 indicates stiffness ratios K_n/K_S in the range 10-300. Values are clearly stress dependent, the greatest anisotropy occurring under low stress.

By comparison the assumption of isotropic elastic properties in the finite element solution means that the ratio of E modulus and shear modulus (G) is usually in the range 2-3, according to equation 5.

$$G = \frac{E}{2(1 + \nu)} \quad \dots\dots\dots (5)$$

As will be seen shortly the above stress dependency of K_n/K_S is clearly reflected in the relative behaviour of the physical and numerical models. Comparison is often good in the case of excavations performed under high horizontal stress levels ($\sigma_h > \sigma_v$, "tectonic"). However under moderate stress levels ($\sigma_h = \sigma_v$, "hydrostatic") the deformations recorded in the physical model greatly exceed the few millimetres predicted by the elastic model.

MODEL LOADING, EXCAVATION AND DEFORMATION

Figure 1 illustrates the loading frame used for applying horizontal stress. The latter was either "hydrostatic" with $\sigma_h = \sigma_v$, or "tectonic" with $\sigma_h > \sigma_v$. The high stress was obtained by elevating both the position and pressure of the "bellow-frame" pistons to give a trapezoidal stress distribution. A theoretical surface intercept of horizontal stress of approximately 8 MPa (full scale) is obtained in this case. At the full simulated depth of 250 metres the horizontal stress is approximately 22 MPa.

The above *hydrostatic* and *tectonic* stress distributions are designed to correspond to two of the three typically observed stress distributions (10). The high values of stress anisotropy for the case

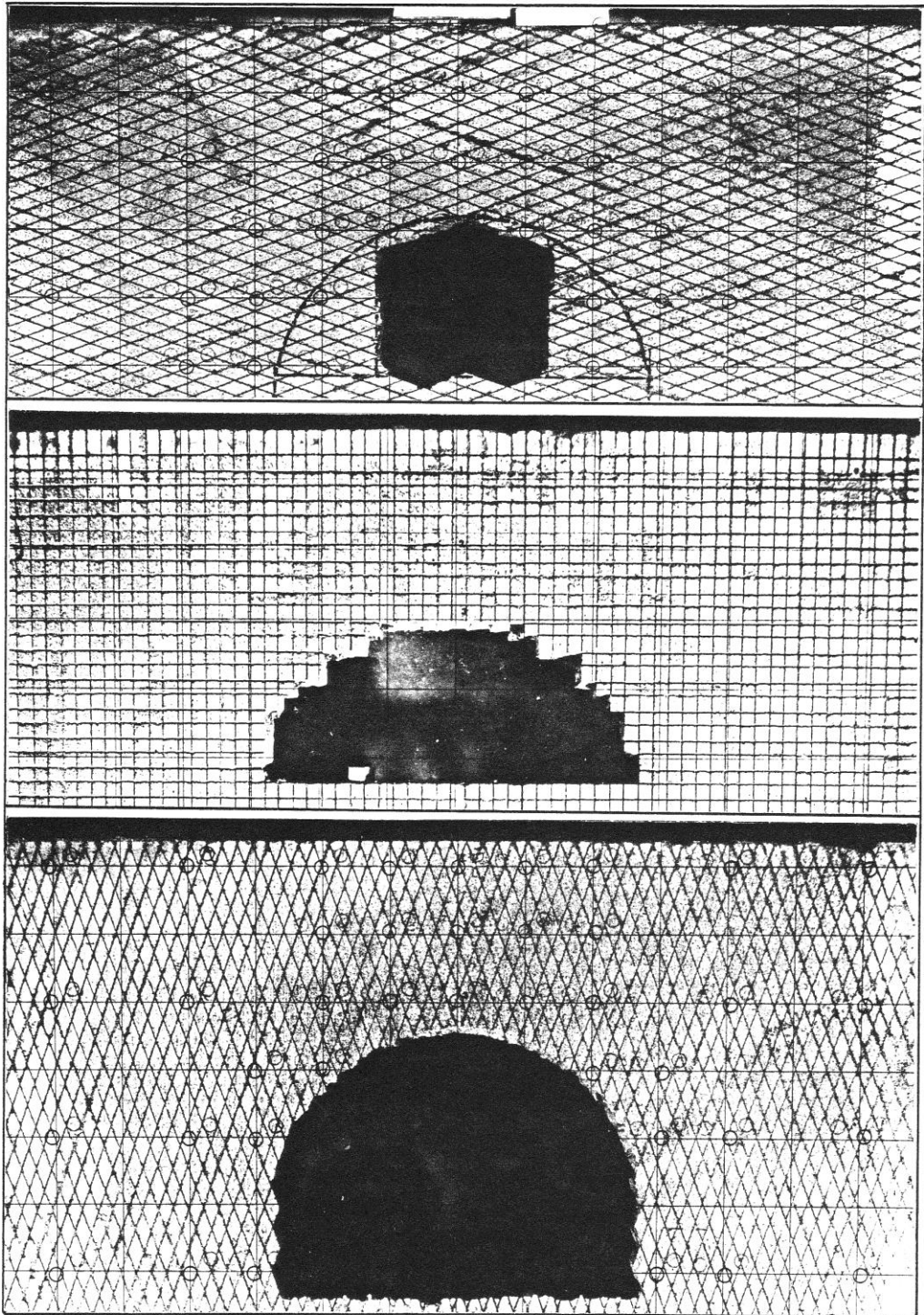


Fig. 6. Models of 20 m and 50 m spans, with various joints systems.

$\sigma_h > \sigma_v$ (*tectonic*) are quite consistent with trends found by Brown and Hoek (11) in one of the most recent surveys of world-wide stress measurements. The ratio of $\sigma_h/\sigma_v = k$ is shown to generally lie between the following limits:

$$100/Z + 0.3 \leq k \leq 1500/Z + 0.5 \quad \dots\dots\dots (6)$$

where Z = depth in metres.

The above anisotropy causes high shearing stresses to be generated on joints not orientated parallel to the vertical and horizontal principal stress directions. This sometimes causes deformation magnitudes and directions to vary widely between differently jointed models.

Figure 6 illustrates some of the single cavern models. Excavation (from a top heading) does not begin until the models have been consolidated under horizontal and vertical (gravity) stress for many hours.

This was found to be necessary to allow the more than 20000 model rock blocks to "shuffle" into intimate contact appropriate to the stress level applied. This consolidation physically takes time; in a joint element F.E. analysis the same process takes a large number of iterations, even when only a few hundred blocks are simulated.

The loading beams are locked in position before excavation. The 30 mm square grid visible on the inside of the glass wall supporting the models is used as a static reference datum for photogrammetric analysis of the stage-by-stage deformations.

Figures 7, 8, and 9 show examples of deformations measured on single cavern models. Four different joint patterns are represented, and stress levels are either "hydrostatic" ($\sigma_h = \sigma_v$, left hand figures) or "tectonic" ($\sigma_h > \sigma_v$, right hand figures).

COMPARISON OF DISCONTINUUM AND CONTINUUM MODELS

Figure 10 indicates the deformation vectors obtained from a two-dimensional *plane stress* analysis, using the finite element method. The assumed elastic constants are shown in the figure. Since deformation magnitudes are directly proportional to the value of E assumed, the computed vectors can be scaled in the ratio $14000/E(\text{actual})$, if other deformation moduli are of interest.

It should be noted that two-dimensional *plane stress* models produce deformations larger than experienced in the case of *plane strain* or three-dimensional models. When jointing is modelled in two-dimensions, this conservatism is increased, since joints striking parallel to the long axis of excavations are known to result in large deformations (12). However, the present *plane stress* numerical and physical models should

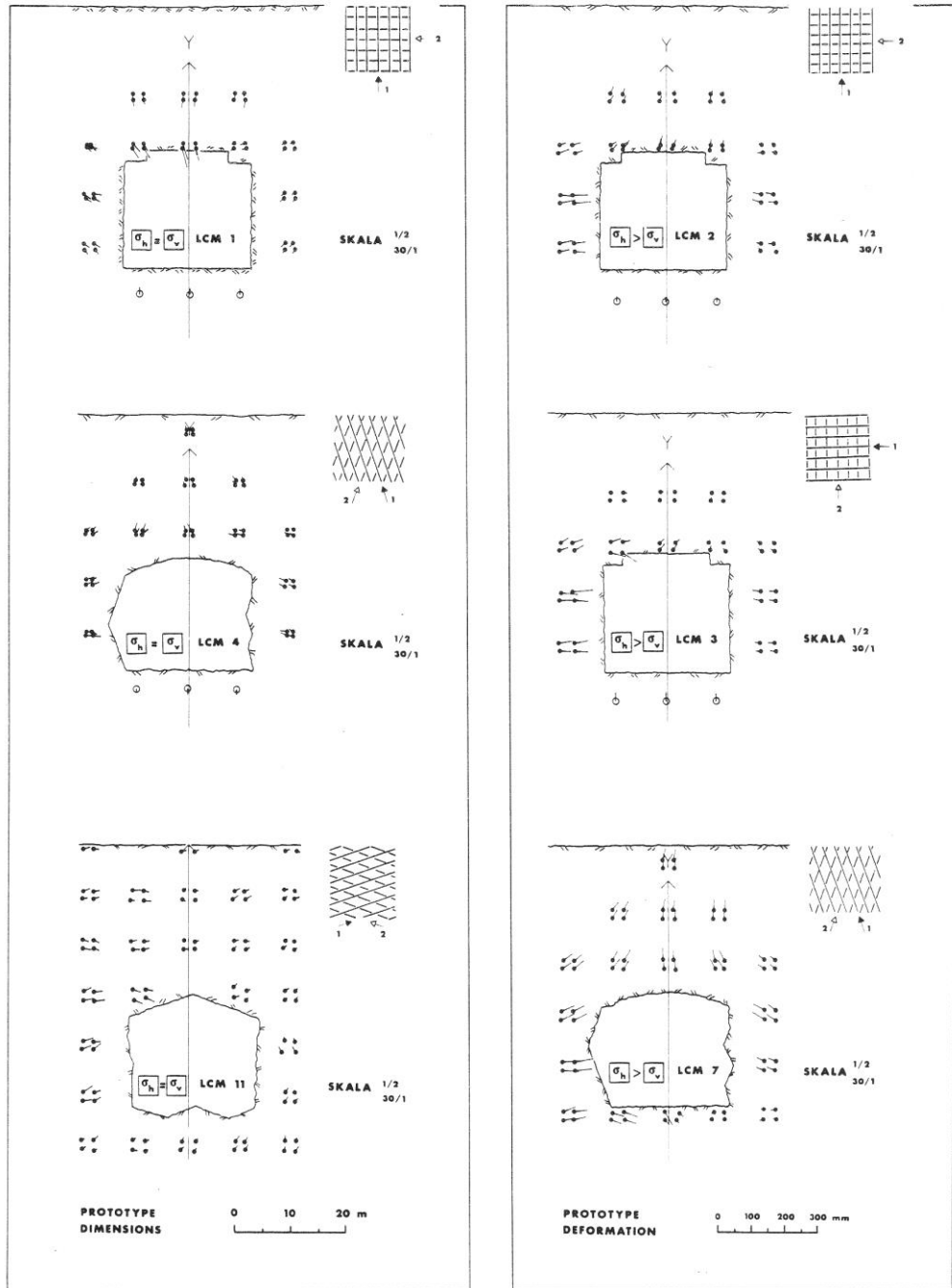


Fig. 7. Deformation vectors for models of 20 m spans. Hydrostatic stress (L.H.S. models), tectonic stress (R.H.S. models). Four types of jointing are indicated.

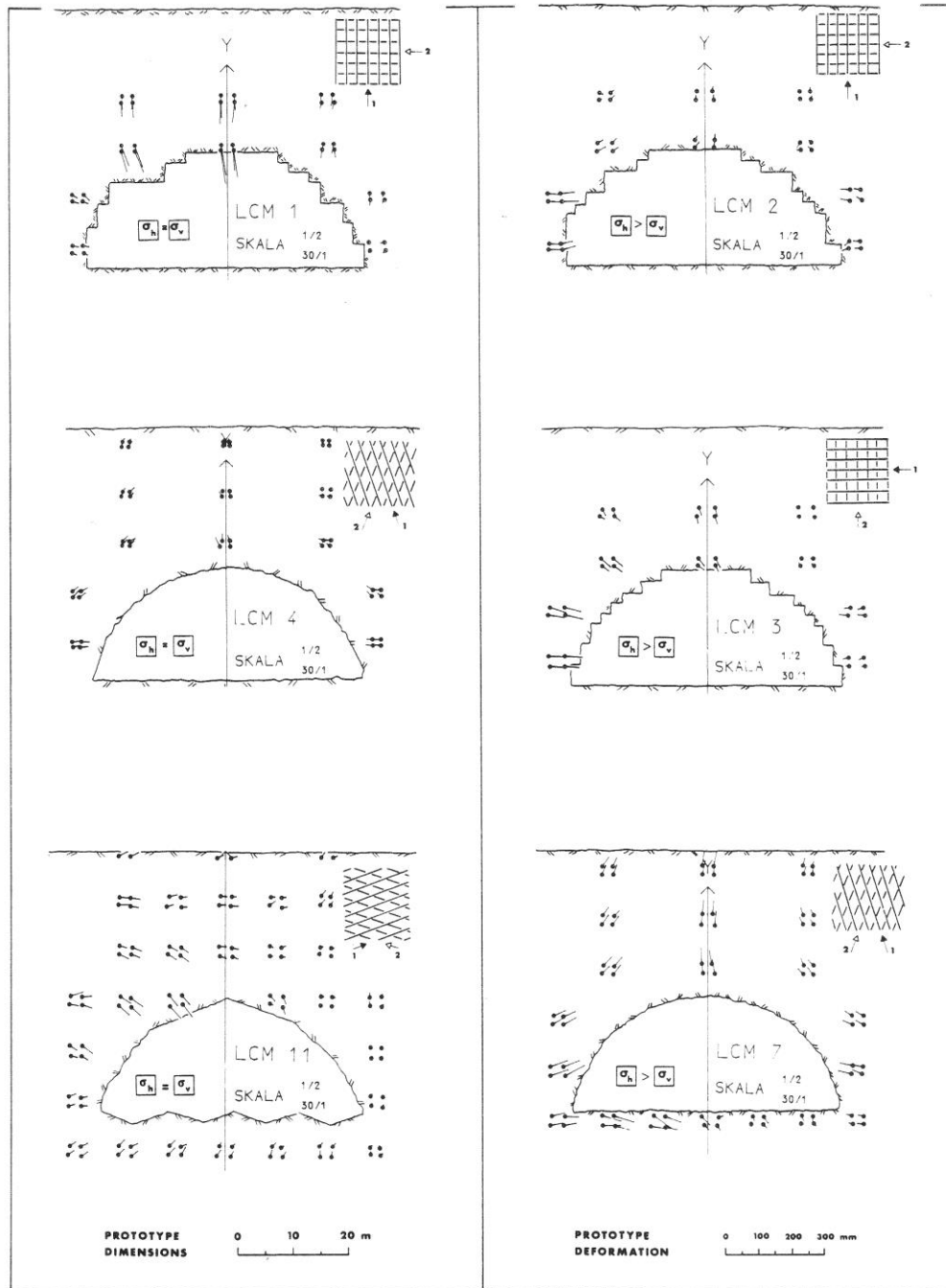


Fig. 8. Deformations obtained when spans are increased to represent 50 m. (Arch radius approx. 25 m, height approx. 20 m).

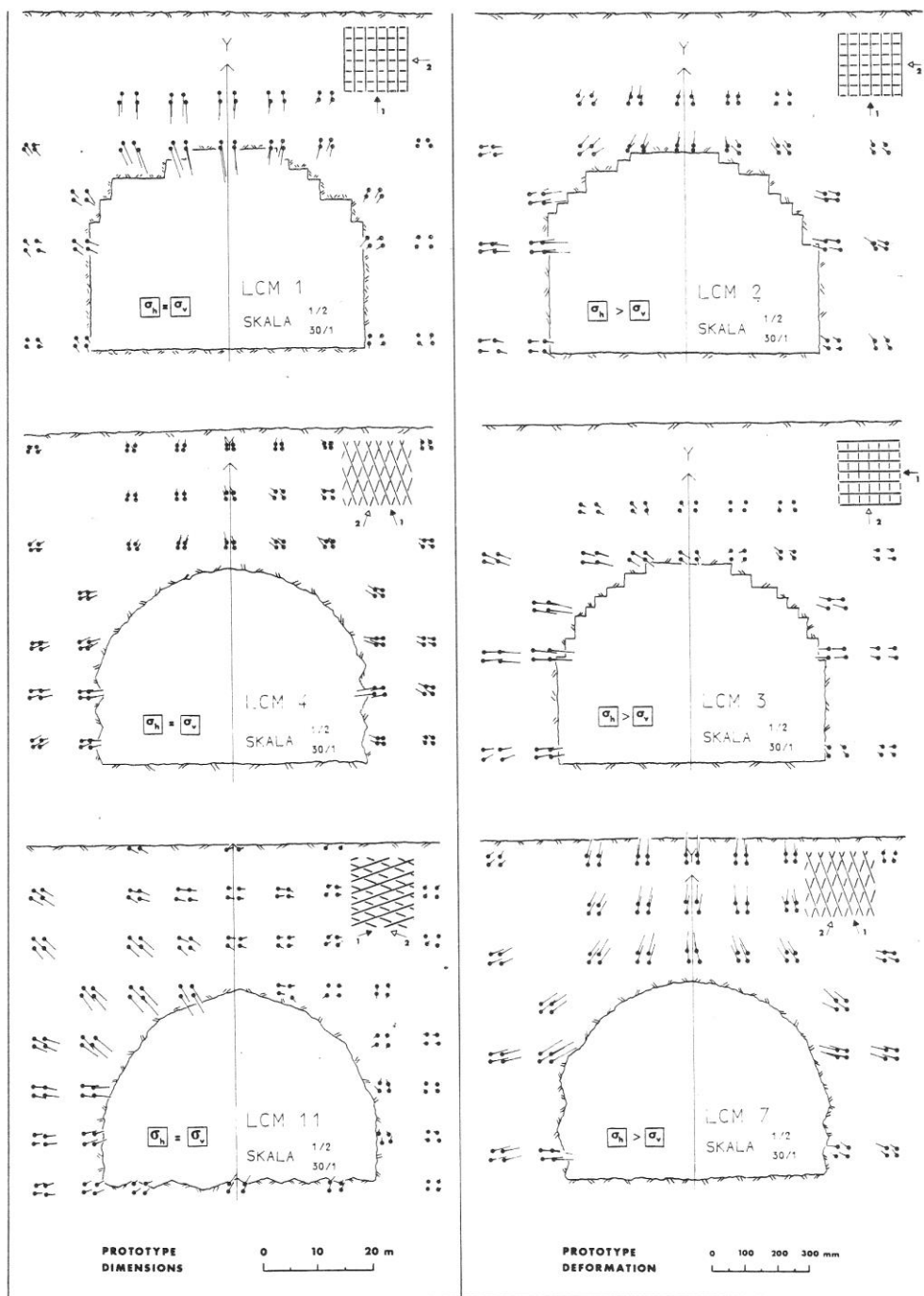


Fig. 9. Deformations obtained from bench excavation, giving a simulated cavern height of 35 metres. Note increased surface heave of LCM 2, LCM 4 and LCM 7.

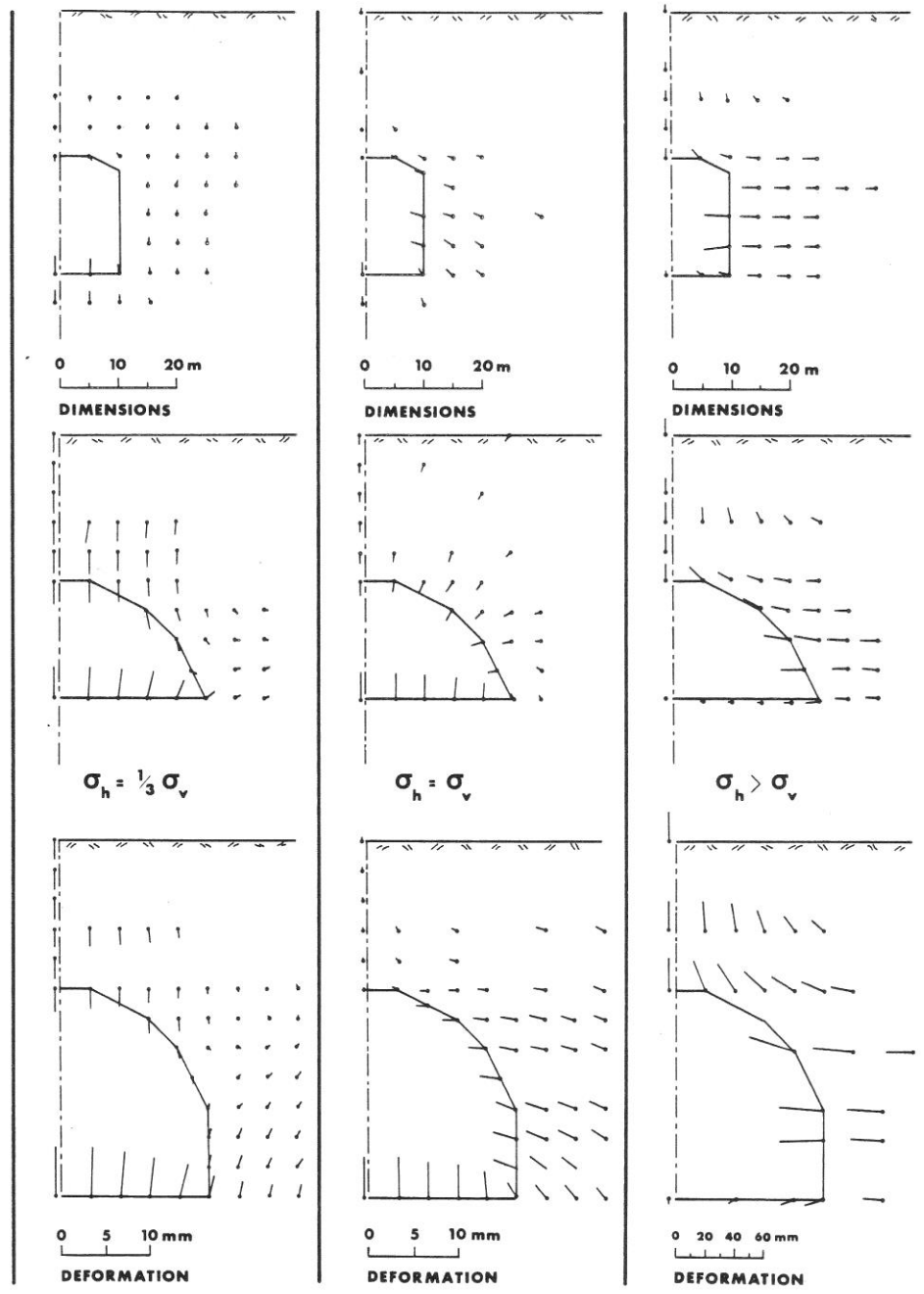


Fig. 10. Deformation vectors computed with linear elastic material properties using the finite element method. ($E = 14,000 \text{ MPa}$, $\rho = 25 \text{ kN/m}^3$, $\nu = 0.1$) $\sigma_h = \sigma_v$ and $\sigma_h > \sigma_v$ as jointed models.

both give the same deformation magnitudes, if it were possible to represent the effect of jointing by a single deformation modulus.

The choice of Poisson's ratio of 0.1 was dictated by the porous nature of the model *material*. The stress dependent shape and volume changes of a *jointed* medium shown in Table 5, suggest that jointing effects might be partly accounted for in continuum models by incorporating a stress dependent Poisson's ratio. For certain large strain problems it would apparently be advantageous to consider a formulation that allowed a "psuedo" Poisson's ratio > 0.5 to be simulated.

Some interesting parameter studies by Dowding (13) using a two-dimensional plane *strain* F.E. analysis, indicated that large variations of Poisson's ratio ν (0.1-0.45) appreciably effected the deformation in the arch of shallow openings. The arch and free surface tended to rise more with low values of ν , due to the smaller increase of stress in the hypothetical third dimension. In contrast, the present physical and F.E. models were both under plane *stress* conditions. The low value of ν (0.1) used in these F.E. analyses will therefore have resulted in smaller heave of the arch (under tectonic stress) than would have been the case if a high value of (ν) had been used.

Both the elastic models and the jointed models have illustrated that underground openings excavated near the surface may exhibit heave or deformation directed upwards towards the free surface. A necessary condition is that the horizontal stresses are at least equal to or greater than the vertical stress. The tendency increases when the depth below surface is of the same order or less than the span width.

In general the jointed models behaved in a more elastic manner when horizontal stresses were high than when hydrostatic. The degree of elastic behaviour increased if the high stress had the effect of closing joints (K_n/K_s similar to E/G) rather than putting them in a state of shear. Models with orthogonal (horizontal and vertical) jointing tended to exhibit elastic behaviour in the arch only when the higher strength (stepped) secondary jointing was horizontal. Horizontal joints in the arch may isolate the immediate roof from the heave effect seen in the overlying rock mass.

Careful study of the effects of increasing the span of single model openings from a simulated 20 m to 50 m indicates few deleterious effects on stability or deformation when horizontal stress is high. The same may be concluded about elastic behaviour (Figure 10). However, two of the jointed models under hydrostatic stress did show increased settlement of the arch when the span was increased. This is also consistent with elastic behaviour, though was exaggerated.

Parallel openings.

The effect of excavating openings in parallel such that the second opening influences the pre-existing opening has often been the subject

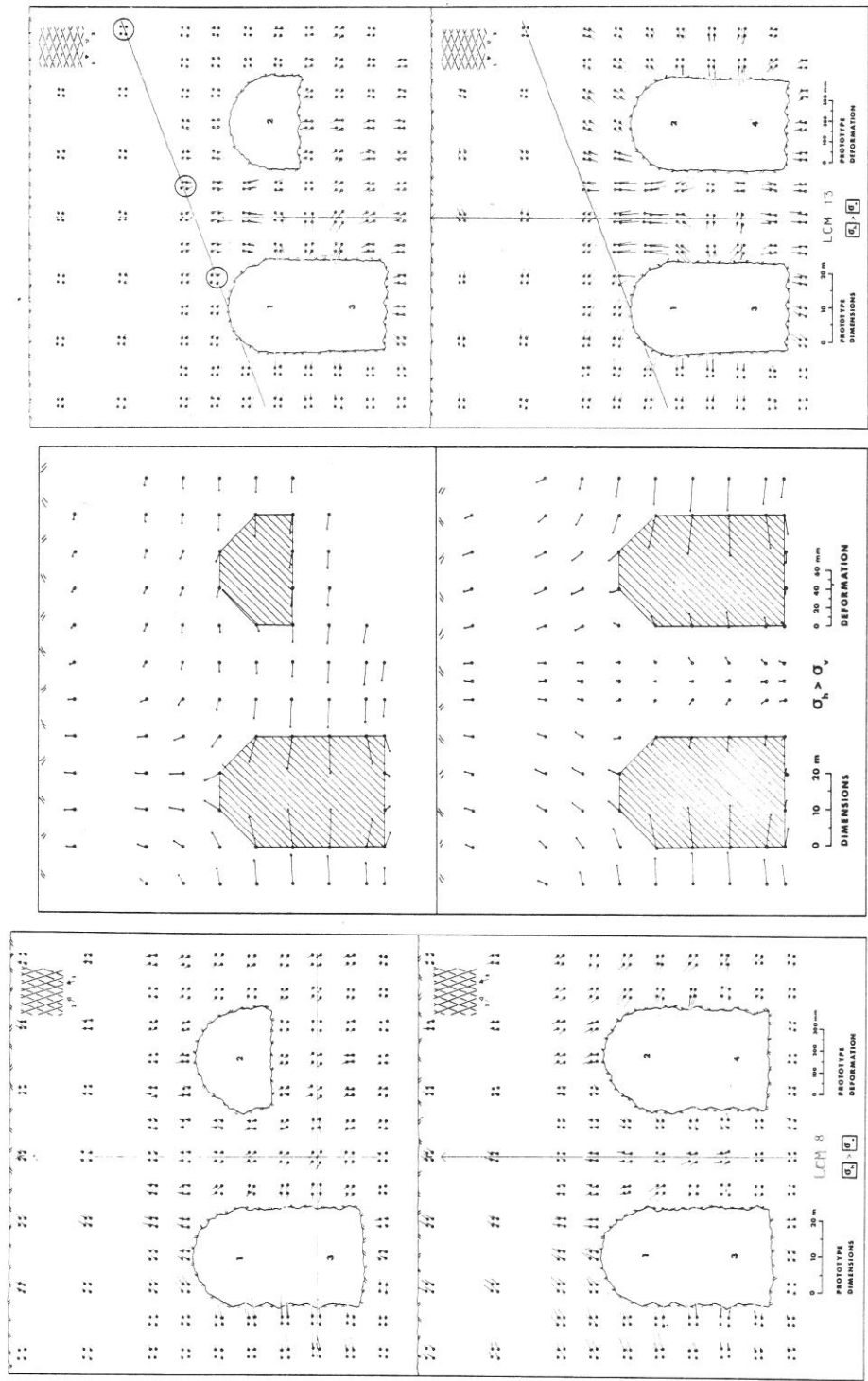


Fig. 11. Comparison of deformation vectors for parallel openings excavated in model rock masses with different joint orientations. Centre figure shows the linear elastic finite element results. All three cases are under the same *tectonic* stress.

of elastic analysis and measurement. Figure 12 shows the results from two model studies, and in the centre, the continuum behaviour obtained from finite element analysis. Comparison of results is most interesting. In the case of the isotropic continuum, deformations naturally become symmetrical about the centre of the pillar when the second opening is completed. Before this symmetrical pattern is reached a net reversal of deformations of up to 35 mm occurs as a result of "benching" in the adjacent opening. By comparison the physical models show relatively little elastic reversal, deformation patterns tend to be directed towards the *last* excavation, rather than strongly influenced by the *next* excavation. This "insensitivity" was particularly marked in model studies of four parallel openings excavated one after the other (14). Presumably one of the reasons for this non-elastic response is the hysteretic behaviour illustrated in Figure 5. Stiffness of joints is higher when *unloading* than when loading. Stress changes are poorly propagated across unloaded parts of a rock mass.

The two physical models illustrated in Figure 12 show significant differences in behaviour due to the contrasting effects of high horizontal stress on the differently orientated jointing. In the model with steeply dipping joints, arch action is good, the pillar is in tension, and the ratio K_n/K_s is not significantly different from E/G - hence the elastic type of behaviour. These conditions are exactly reversed in the model with gently dipping joints. (Note the "faulting event" in this model. Increasing shear stresses caused increased displacement on one of the gently dipping joints as "benching" was being completed.)

The elastic type of response to high horizontal stress which tends to put pillars in tension has also been observed in some room and pillar mines. Horizontal cracks in pillars under tension have been reported from the Tyrtyri limestone mine in Finland. Removal of the pillars improved stability despite greatly increased spans (15). Maximum horizontal stresses were in the range 14 to 17 MPa, exactly comparable with the present models.

Comparable experiences are reported at Skorovas mine in Norway (16). Removal of unstressed ore pillars resulted in slight *upward* deformation (2-3 mm) of the new arch despite the large spans created (66 m). At both the above mines, single unsupported rooms with spans of up to 80-100 metres are already in existence or planned. Depths below surface range from about 40 to 100 m in both cases.

DYNAMIC LOADING EFFECTS

A review of damage to tunnels caused by earthquakes (17), reveals that unlined tunnels generally do not experience any block falls until peak surface accelerations and velocities exceed about 0.2 g and 20 cm/sec. respectively. Severe damage involving major rock falls may occur in poor ground or in portal areas when surface motions exceed

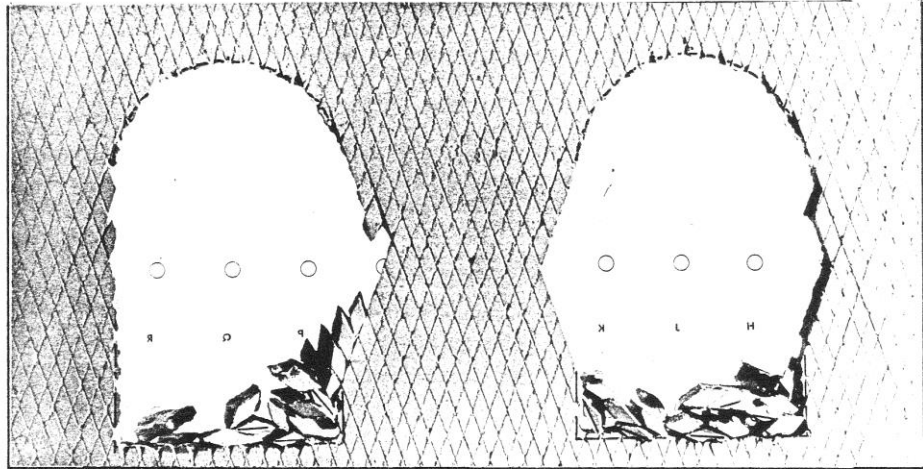


Fig. 12. Progressive collapse of model (see Fig. 1) during dynamic loading of few seconds duration.

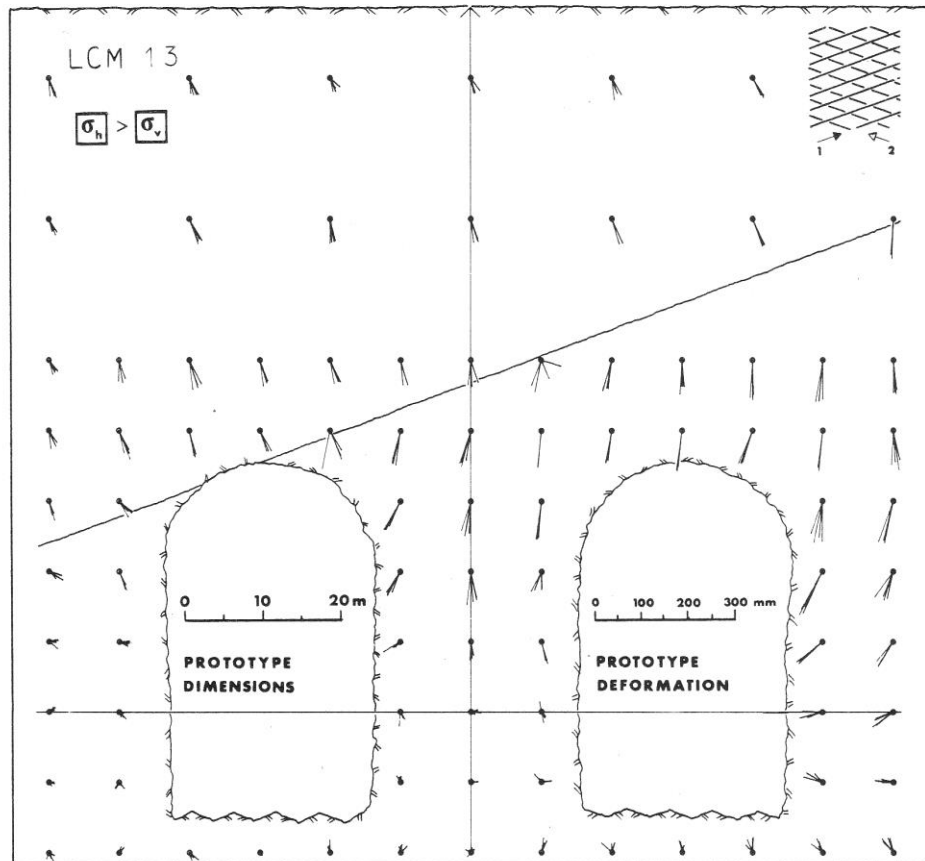


Fig. 13. Deformation caused by dynamic loading showing increased displacement along the "faulted" joint.

0.5 g and 80 cm/sec. The performance of *large near-surface* caverns is therefore of some interest.

Acceleration magnitudes reached in model dynamic loading tests were registered in a model instrumented with two small accelerometers embedded and cemented close to the surface (ca. 5-10 m simulated depth). The accelerometers were of similar density to the model material and were set to register both horizontal and vertical motion in the plane of the model. The acceleration signals were recorded on a multi-channel tape recorder and were integrated to produce velocity and displacement magnitudes. The peak values recorded in the horizontal direction are given in Table 6. The few seconds duration of the dynamic loading tests corresponds to a full scale duration of the order of 1 minute. Magnitudes expected "in practice" represent the approximate range for severe earthquakes calculated at rock sites in the neighbourhood of causative faults (18, 19).

TABLE 6. Model and prototype "earthquake" magnitudes.

	MODEL	PROTOTYPE	PRACTICE
Acceleration	0.2-0.7 g	0.2-0.7 g	0.1-0.7 g
Velocity	1.0-5.0 cm/s	15-90 cm/s	10-200 cm/s
Displacement	0.02-0.1 cm	6-30 cm	1-30 cm
Frequency	7-200 Hz	0.4-12 Hz	0.5-10 Hz

(Velocity and time scaling: $\lambda^{1/2}$, displacement scaling: λ)

Figure 12 illustrates the final state of collapse of one of the models of parallel openings. The block falls occurred progressively during the few seconds duration of the test. By comparison the model with gently dipping joints suffered no block falls, merely a general settlement in the neighbourhood of the openings, as shown in Figure 13. Deformation caused by dynamic loading was of similar magnitude to that caused by excavation. The three different types of models studied (single large opening, two parallel openings, four parallel openings (14) showed little if any settlement below the base of the openings as a result of dynamic loading. Yet in each case there was approximately 150 metres of simulated rock mass beneath the openings which might have been expected to consolidate during the shaking. It appears that the zone around the openings that is sensitive to dynamic (i.e. cyclic) loading is more or less the same zone that undergoes deformation during excavation under "static" conditions. The disturbance of the virgin stress caused by excavation causes a sufficient increase in the ratio τ/σ_n along individual joints (due to increased shear and reduced normal stress) that they are locally susceptible to progressive accumulation of shear displacement (fatigue) from a small number of cycles. The number of cycles required to cause settlements in the undisturbed model rockmass would be far in excess of the few tens of significant cycles resulting from the model earthquakes.

ACKNOWLEDGEMENTS

The research described in this paper has been sponsored by the Royal Norwegian Council for Scientific and Industrial Research (NTNF) and by the Swedish State Power Board (SV) as part of BeFo project 21. This support is gratefully acknowledged.

REFERENCES

- (1) Eristov, V.S. and Khechinov, Y.E., Effect of Excavation by Stages on the Stress and Strain on Structures of the Underground Generator Rooms of Hydroelectric Stations. Hydrotechnical Construction, No. 7, 1972, pp. 637-649.
- (2) Imrie, A.S. and Jory, L.T., Behaviour of the Underground Powerhouse Arch at the W.A.C. Bennett Dam during Excavation. Canadian Rock Mechanics Symposium, 5. Toronto 1968. Proceedings, 1969, pp. 19-37.
- (3) Judd, W.R. and Perloff, W.H., Predicted and Measured Displacements for Tunnels. American Society of Civil Engineers. Symposium or Underground Rock Chambers. Phoenix, Ariz. 1971. Proceedings, 1972, pp. 487-514.
- (4) Goodman, R.E. Methods of Geological Engineering in Discontinuous Rocks. St. Paul, a.o.pl., West Publ., 1976, 472 p.
- (5) Cundall, P., Marti, J., Beresfort, P., Last, N., Asgian, M. and Maini, T., Computer Modelling of Jointed Rock Masses. Waterways Experiment Station, Vicksburg, Miss. Technical report, N-78,4. 1978, 396 p.
- (6) Groth, T. and Jonasson, P., FEM-analys jämförd med modellstudier. (FEM-Analysis Compared to Model Studies). Rock Mechanics Meeting, Stockholm 1978. Papers, pp. 119-136.
- (7) Barton, N., A Low Strength Material for Simulation of the Mechanical Properties of Intact Rock in Rock Mechanics Models. International Society for Rock Mechanics. 2nd Congress, Belgrade 1970. Proceedings, Vol. 2, paper, 3-15.
- (8) Barton, N., A Model Study of Rock-Joint Deformation. International Journal of Rock Mechanics and Mining Sciences, Vol. 9, 1972, pp. 579-602.
- (9) Barton, N. and Choubey, V., The shear strength of rock joints in theory and practice. Rock Mechanics, Vol. 10, No. 1/2, 1977 pp. 1-54.
- (10) Herget, G., Variation of Rock Stresses with Depth at a Canadian Iron Mine. International Journal of Rock Mechanics and Mining Sciences, Vol. 10, No. 1, 1973, pp. 37-51.

(11) Brown, E.T. and Hoek, E., Trends in Relationships Between Measured In-situ Stresses and Depth. International Journal of Rock Mechanics and Mining Sciences & Geomechanics Abstracts, Vol. 15, 1978, pp. 211-215.

(12) Cording, E.J., Hendron, A.J. and Deere, D.U., Rock Engineering for Underground Caverns. American Society of Civil Engineers. 1972. Symposium on Underground Rock Chambers. Phoenix, Ariz. 1971, pp. 567-600

(13) Dowding, C., Finite Element Model Study of the Relative Construction Difficulty of Machine Halls and Tunnels. Norwegian Geotechnical Institute, Internal Report 54201-2, April 1972, pp. 1-76.

(14) Barton, N., Physical Model Studies of Large Span Underground Openings. Rock Mechanics Meeting. Stockholm 1978. Papers, pp. 95-117.

(15) Matikainen, R., Bergmekaniska Mätningar i Finland. (Rock Mechanical Investigations in Finland). Fjellsprengningsteknikk 1973 - Bergmekanikk 1973. Lecture. Trondheim, Tapir, 1974, pp. 16.1-16.15.

(16) Haugen, A. and Myrvang, A., Store Brytningsrom ved Skorovas Gruber. (Large Excavation Rooms at the Skorovas Mines). Fjellsprengningsteknikk 1974 - Bergmekanikk 1974. Lecture. Trondheim, Tapir, 1975, pp. 19.1-19.10.

(17) Dowding, C. and Rozen, A., Damage to Rock Tunnels from Earthquake Shaking. American Society of Civil Engineers. Proceedings, Vol. 104, No. GT 2, 1978, pp. 175-191.

(18) Schnabel, P.B. and Seed, H.B., Accelerations in Rock for Earthquakes in the Western United States. Seismological Society of America. Bulletin, Vol. 63, No. 2, 1973, pp. 501-516.

(19) Chang, F.K., State-of-the-art for Assessing Earthquake Hazards in the United States. Report 9. Catalogues of strong motion earthquake records. Vol. I. Western United States, 1933-1971, Waterways Experiment Station, Vicksburg, Vicksburg, Miss. Miscellaneous paper, S-73-1. 1978, Var. pag.

